54. Perovic S, Pergande G, Ushijima H, Kelve M, Forrest J, Muller WE (1995) Flupirtine partially prevents neuronal injury induced by prion protein fragment and lead acetate. Neurodegeneration 4:369-374
55. Perovic S, Schleger C, Pergande G, Iskric S, Ushijima H, Rytik P, Muller WE (1994) The triaminopyridine flupirtine prevents cell death in rat cortical cells induced by N-methyl-D-aspartate and gp120 of HIV-1. Eur J Pharmacol 288:27-33
56. Otto M, Cepek L, Ratzka P, Doehlinger S, Boekhoff I, Wiltfang J, Irle E, Pergande G, Ellers-Lenz B, Windl O, Kretzschmar HA, Poser S, Prange H (2004) Efficacy of flupirtine on cognitive function in patients with CJD: A double-blind study. Neurology 62:714-718
57. Enari M, Flechsig E, Weissmann C (2001) Scrapie prion protein accumulation by scrapie-infected neuroblastoma cells abrogated by exposure to a prion protein antibody. Proc Natl Acad Sci USA 98,9295-9299
58. Sigurdsson EM, Brown DR, Daniels M, Kascsak RJ, Kascsak R, Carp R, Meeker HC, Frangione B, Wisniewski T (2002) Immunization delays the onset of prion disease in mice. Am J Pathol 161:13-17
59. Gilch S, Wopfner F, Renner-Muller I, Kremmer E, Bauer C, Wolf E, Brem G, Groschup MH, Schatzl HM (2003) Polyclonal anti-PrP auto-antibodies induced with dimeric PrP interfere efficiently with PrPSc propagation in prion-infected cells. J Biol Chem 278:18524-185231
60. Heppner FL, Musahl C, Arrighi I, Klein MA, Rulicke T, Oesch B, Zinkernagel RM, Kalinke U, Aguzzi A (2001) Prevention of scrapie pathogenesis by transgenic expression of anti-prion protein antibodies. Science 294:178-182
61. Peretz D, Williamson RA, Kaneko K, Vergara J, Leclerc E, Schmitt-Ulms G, Mehlhorn IR, Legname G, Wormald MR, Rudd PM, Dwek RA, Burton DR, Prusiner SB (2001) Antibodies inhibit prion propagation and clear cell cultures of prion infectivity. Nature 412:739-743
62. White AR, Enever P, Tayebi M, Mushens R, Linehan J, Brandner S, Anstee D, Collinge J, Hawke S (2003) Monoclonal antibodies inhibit prion replication and delay the development of prion disease. Nature 422:80-83
63. Doh-Ura K, Iwaki T, Caughey B (2000) Lysosomotropic agents and cysteine protease inhibitors inhibit scrapie-associated prion protein accumulation. J Virol 74:4894-4897
64. Korth C, May BC, Cohen FE, Prusiner SB (2001) Acridine and phenothiazine derivatives as pharmacotherapeutics for prion disease. Proc Natl Acad Sci USA 98:9836-9841
65. Turnbull S, Tabner BJ, Brown DR, Allsop D (2003) Quinacrine acts as an antioxidant and reduces the toxicity of the prion peptide PrP106-126. Neuroreport 14:1743-1745
66. Collins SJ, Lewis V, Brazier M, Hill AF, Fletcher A, Masters CL (2002) Quinacrine does not prolong survival in a murine Creutzfeldt-Jakob disease model. Ann Neurol 52:503-506
67. Barret A, Tagliavini F, Forloni G, Bate C, Salmona M, Colombo L, De Luigi A, Limido L, Suardi S, Rossi G, Auvre F, Adjou KT, Sales N, Williams A, Las-

mezas C, Deslys JP (2003) Evaluation of quinacrine treatment for prion diseases. J Virol 77:8462-8469
68. Nakajima M, Yamada T, Kusuhara T, Furukawa H, Takahashi M, Yamauchi A, Kataoka Y (2004) Results of quinacrine administration to patients with Creutzfeldt-Jakob disease. Dement Geriatr Cogn Disord 17:158-163
69. http://www.ctu.mrc.ac.uk/studies/cjd.asp
70. Diringer H, Ehlers B (1991) Chemoprophylaxis of scrapie in mice. J Gen Virol 782:457-460
71. Caughey B (1994) Protease-resistant PrP accumulation and scrapie agent replication: a role for sulphated glycosoaminoglycans? Biochem Neurodegen Disord 22:163-167
72. Caughey B, Brown K, Raymond GJ, Katzenstein GE, Thresher W (1994) Binding of the protease-sensitive form of PrP (prion protein) to sulfated glycosaminoglycan and congo red. J Virol 68:2135-2141
73. Caughey B, Raymond G (1993) Sulfated polyanion inhibition of scrapie associated PrP accumulation in cultured cells. J Virol 67:643-650
74. Perez M, Wandosell F, Colaco C, Avila J (1998) Sulphated glycosaminoglycans prevent the neurotoxicity of a human prion protein fragment. Biochem J 335:369-374
75. Farquhar C, Dickinson A (1986) Prolongation of scrapie incubation period by an injection of dextran sulphate 500 within the month before of after infection. J Gen Virol 67:463-473
76. Ehlers B, Diringer H (1984) Dextran sulphate 500 delays and prevents mouse scrapie by impairment of agent replication in spleen. J Gen Virol 65:1325-1330
77. Kimberlin RH, Walker CA (1988) Pathogenesis of experimental scrapie. Ciba Found Symp 135:37-62
78. Ladogana A, Casaccia P, Ingrosso L, Cibati M, Salvatore M, Xi YG, Masullo C, Pocchiari M (1992) Sulphate polyanions prolong the incubation period of scrapie infected hamsters. J Gen Virol 73:661-665
79. Farquhar C, Dickinson A, Bruce M (1999) Prophylactic potential of pentosan polysulphate in transmissible spongiform encephalopathies. Lancet 353:117
80. Doh-ura K, Ishikawa K, Murakami-Kubo I, Sasaki K, Mohri S, Race R, Iwaki T (2004) Treatment of transmissible spongiform encephalopathy by intraventricular drug infusion in animal models. J Virol 78:4999-5006
81. Dawes J, Prowse CV, Pepper DS (1986) Absorption of heparin, LMW heparin and SP54 after subcutaneous injection, assessed by competitive binding assay. Thromb Res 44:683-693
82. Dawes J, Pepper DS (1992) Human vascular endothelial cells catabolise exogenous glycosaminoglycans by a novel route. Thromb Haemost 67:468-472
83. McGregor IR, Dawes J, Pepper DS (1985) Metabolism of sodium pentosan polysulphate in man measured by a new competitive binding assay for sulphated polysaccharides - comparison with effects upon anticoagulant activity, lipolysis and platelet A-granule proteins. Thromb Haemost 53:411-414
84. Sie P, Albarede JL, Robert M, Bouloux C, Lansen J, Chigot C, Correll S, Thouvenot JP, Boneu B (1986) Tolerance and biological activity of pentosan

polysulphate after intramuscular or subcutaneous administration for ten days in human volunteers. Thromb Haemost 55:86-89
85. Mulholland SG, Hanno P, Parsons CL, Sant GR, Staskin DR (1990) Pentosan polysulfate sodium for therapy of interstitial cystitis. A double-blind placebo-controlled clinical study. Urology 35:552-558
86. Tardy-Poncet B, Tardy B, Grelac F, Reynaud J, Mismetti P, Bertrand JC, Guyotat D (1994) Pentosan polysulfate induced thrombocytopaenia and thrombosis. Am J Haematol 45:252-257
87. Emmett CJ, Stewart GR, Johnson RM, Aswani SP, Chan RL, Jakeman LB (1996) Distribution of radioiodinated recombinant human nerve growth factor in primate brain following intracerebroventricular infusion. Exp Neurol 140:151-160
88. Gill SS, Patel NK, Hotton GR, O'Sullivan K, McCarter R, Bunnage M, Brooks DJ, Svendsen CN, Heywood P (2003) Direct brain infusion of glial cell line-derived neurotrophic factor in Parkinson disease. Nat Med 9:589-595
89. Cornford EM (1985) The blood-brain barrier, a dynamic regulatory interface. Mol Physiol 7:219-260
90. Neuwelt EA (2004) Mechanisms of disease: the blood-brain barrier. Neurosurgery 54:131-142
91. Kroll RA, Neuwelt EA (1998) Outwitting the blood-brain barrier for therapeutic purposes: osmotic opening and other means. Neurosurgery 42:1083-1100
92. Kemper EM, Boogerd W, Thuis I, Beijnen JH, van Tellingen O (2004) Modulation of the blood-brain barrier in oncology: therapeutic opportunities for the treatment of brain tumours? Cancer Treat Rev 30:415-423
93. Pakulski C, Dybkowska K, Drobnik L (1998) [Brain barriers. Part II. Blood/cerebrospinal fluid barrier and cerebrospinal fluid /brain tissue barrier]. Neurol Neurochir Pol 32:133-139
94. Fossan G, Cavanagh ME, Evans CA, Malinowska DH, Mollgard K, Reynolds ML, Saunders NR (1985) CSF-brain permeability in the immature sheep fetus: a CSF-brain barrier. Brain Res 350:113-124
95. Czosnyka M, Czosnyka Z, Momjian S, Pickard JD (2004) Cerebrospinal fluid dynamics. Physiol Meas 25:R51-76
96. Fenstermacher JD, Ghersi-Egea JF, Finnegan W, Chen JL (1997) The rapid flow of cerebrospinal fluid from ventricles to cisterns via subarachnoid velae in the normal rat. Acta Neurochir Suppl 70:285-287
97. Abbott NJ (2004) Evidence for bulk flow of brain interstitial fluid: significance for physiology and pathology. Neurochem Int 45:545-552
98. Todd NV, Morrow J, Doh-ura K, Dealler S, O'Hare S, Farling P, Duddy M, Rainov NG (2004) Cerebroventricular infusion of pentosan polysulphate in human variant Creutzfeldt-Jakob disease. J Infect - in press

Brief Communication

Quinoline and Benzimidazole Derivatives: Candidate Probes for *In Vivo* Imaging of Tau Pathology in Alzheimer's Disease

Nobuyuki Okamura,[1,2] Takahiro Suemoto,[1] Shozo Furumoto,[3] Masako Suzuki,[1] Hiroshi Shimadzu,[1] Hiroyasu Akatsu,[4] Takayuki Yamamoto,[4] Hironori Fujiwara,[5] Miyako Nemoto,[6] Masahiro Maruyama,[6] Hiroyuki Arai,[5] Kazuhiko Yanai,[2] Tohru Sawada,[1] and Yukitsuka Kudo[1,3]

[1]BF Research Institute, Osaka 541-0045, Japan, [2]Department of Pharmacology, Tohoku University Graduate School of Medicine, Sendai 980-8575, Japan, [3]Tohoku University Biomedical Engineering Research Organization, Sendai 980-8575, Japan, [4]Choju Medical Institute, Fukushimura Hospital, Toyohashi 441-8124, Japan, and Departments of [5]Geriatric and Complementary Medicine and [6]Geriatric and Respiratory Medicine, Tohoku University Graduate School of Medicine, Sendai 980-8574, Japan

Neurofibrillary tangles (NFTs), neuropil threads, and neuritic elements of senile plaques predominantly comprise hyperphosphorylated tau protein and represent pathological characteristics of Alzheimer's disease (AD). These lesions occur before the presentation of clinical symptoms and correlate with the severity of dementia. *In vivo* detection of these lesions would thus prove useful for preclinical diagnosis of AD and for tracking disease progression. The present study introduces three novel compounds, 4-[2-(2-benzoimidazolyl)ethenyl]-*N*,*N*-diethylbenzenamine (BF-126), 2-[(4-methylamino)phenyl]quinoline (BF-158), and 2-(4-aminophenyl)quinoline (BF-170), as candidate probes for *in vivo* imaging of tau pathology in the AD brain. When solutions of these compounds are injected intravenously into normal mice, these agents exhibit excellent brain uptake and rapid clearance from normal brain tissue. These compounds display relatively lower binding affinity to β-amyloid fibrils and higher binding affinity to tau fibrils, compared with previously reported probe BF-168. In neuropathological examination using AD brain sections, BF-126, BF-158, and BF-170 clearly visualize NFTs, neuropil threads, and paired helical filament-type neuritis. Autoradiography using ^{11}C-labeled BF-158 further demonstrated labeling of NFTs in AD brain sections. These findings suggest the potential usefulness of quinoline and benzimidazole derivatives for *in vivo* imaging of tau pathology in AD.

Key words: imaging; neuropathology; Aβ peptide; tau; neurofibrillary tangles; paired helical filaments

Introduction

The deposition of senile plaques (SPs) and neurofibrillary tangles (NFTs) represents a pathological hallmark of Alzheimer's disease (AD). Definitive diagnosis of AD relies on the postmortem assessment of these pathological changes. SPs are extracellular deposits containing β-amyloid (Aβ) peptide cleaved from a longer amyloid precursor protein to produce a 40–43 aa peptide. NFTs comprise bundles of paired helical filaments (PHFs) that result from the abnormal aggregation of tau protein (Lee et al., 1991). PHFs accumulate in the neuronal cytoplasm and form NFT with age. Initial lesions of NFTs occur in the transentorhinal cortex, followed by involvement of the entorhinal cortex and hippocampus, progressing to the neocortex (Braak and Braak, 1991). Severity of neurofibrillary pathology correlates with severity of cognitive impairment (Dickson, 1997). However, these pathological changes can be observed in elderly individuals with normal cognition. The pathological process of AD must therefore begin before the presentation of the clinical symptoms of dementia (Price and Morris, 1999). Recent drug development has been aimed at preventing the accumulation of SPs and NFTs in presymptomatic AD patients. The ability to measure levels of these lesions in the living human brain is thus desirable for presymptomatic diagnosis of AD.

Many attempts have been made to visualize AD-specific pathological changes in the living brain (Nordberg, 2004). Currently, the most practical methods for this purpose are to measure the distribution of intravenously administered radiotracers that selectively bind to SPs or NFTs using positron emission tomography (PET) or single photon emission computed tomography. Such radiotracers require sufficient permeability to the blood–brain barrier (BBB). Several researchers have focused on developing lipophilic radiotracers for imaging AD-specific pathology (Shoghi-Jadid et al., 2002; Klunk et al., 2004; Kung et al., 2004; Mathis et al., 2004; Okamura et al., 2004a). To obtain a better understanding of the pathophysiology of AD, individual evaluation of the distributions of Aβ pathology and tau pathology is desirable. However, no surrogate markers exist that allow evaluation of the severity of neurofibrillary pathology in AD brains, because of the difficulty in developing an NFT-specific imaging probe (Small et al., 2002).

We screened >2000 small molecules to develop novel agents

Received May 2, 2005; revised Sept. 26, 2005; accepted Sept. 27, 2005.

This study was supported by the Organization for Pharmaceutical Safety and Research of Japan, the New Energy and Industrial Technology Development Organization, and the Novartis Foundation for Gerontological Research.

Correspondence should be addressed to Yukitsuka Kudo, Tohoku University Biomedical Engineering Research Organization, 2-1, Seiryo-machi, Aoba-ku, Sendai 980-8575, Japan. E-mail: kudoyk@tubero.tohoku.ac.jp.

DOI:10.1523/JNEUROSCI.1738-05.2005

 0270-6474/05/2510857-06$15.00/0

for use in PET with a high affinity for SPs and NFTs. This process has identified novel quinoline and benzimidazole derivatives with a preference to bind NFTs rather than SPs and readily cross the BBB. The present study evaluated whether these compounds may offer a good indicator of tau pathology in AD patients.

Materials and Methods

Preparation of BF compounds. Three novel compounds, 4-[2-(2-benzoimidazolyl)ethenyl]-*N*,*N*-diethylbenzenamine *p*-toluenesulfonate (BF-126), 2-[(4-methylamino)phenyl]quinoline (BF-158), and 2-(4-aminophenyl)quinoline (BF-170), were originally designed by us and custom-synthesized by Tanabe R&D Service (Osaka, Japan) (see Fig. 1*A*). [^{11}C]BF-158 was synthesized from N-Boc-protected BF-170 and [^{11}C]methyl triflate (see Fig. 1*B*). Briefly, to a solution of N-Boc-protected BF-170 and NaH in dry acetone was bubbled thorough [^{11}C]methyl triflate at room temperature, followed by heating at 80°C for 1 min. The reaction was then acidified with a dioxane solution of hydrochloric acids and heated for an additional 5 min. After neutralizing the reaction with sodium phosphate buffer, the crude mixture was purified with semipreparative reverse-phase HPLC to give [^{11}C]BF-158 with a radiochemical purity of >95% and a specific activity of 11–15 GBq/μmol at the end of synthesis. Isolated [^{11}C]BF-158 was solubilized into 40% ethanol solution for *in vitro* autoradiography of AD brain sections and saline with polysorbate 80 for *in vivo* brain-uptake study using normal mice.

Biodistribution of BF compounds in normal mice. Brain uptake after intravenous injection of BF-126 and BF-170 in mice was analyzed using HPLC with a fluorescence detector, as described previously (Okamura et al., 2004b). Briefly, each compound (1 mg/kg), dissolved in diluted HCl, was administered into the tail vein of male Institute of Cancer Research (ICR) mice (7 weeks of age; body weight, 30–40 g; $n = 3$). At 2 and 30 min after the injection of compounds, the brain was removed. Brain homogenates were centrifuged at 14,000 rpm for 10 min, and the supernatant was used for extraction. The mobile phase was 20 mM phosphate buffer, pH 6.5, and acetonitrile at a ratio of 2:3 for BF-126 and 1:1 for BF-170, at a flow rate of 1 ml/min. An FS-8020 fluorescence detector (Tosoh, Tokyo, Japan) was operated at excitation/emission wavelengths of 420/525 nm for BF-126 and 280/500 nm for BF-170. Brain uptake of BF-158 was measured using ^{11}C-labeled compound. [^{11}C]BF-158 (2.6–3.3 MBq) was administered into the tail vein of ICR mice ($n = 12$; male; average weight, 24 g). The mice were then killed by decapitation at 2, 10, 30, and 60 min after injection. The brains were removed and weighted, and the radioactivity was counted with an automatic γ-counter (Wizard 1480; PerkinElmer Wallac, Turku, Finland). The percentage injected dose per gram (%ID/g) was calculated by comparison of tissue count to tissue weight. Each %ID/g value is an average ± SEM of three separate experiments.

In vitro *binding assays.* The dissociation constant (K_d) and maximum specific binding of BF-180 were determined as described previously (Okamura et al., 2004a). For inhibition studies, binding studies were performed using aggregates of synthetic Aβ1–42 (Peptide Institute, Osaka, Japan). A mixture containing 50 μl of BF-126, BF-158, and BF-170, 50 μl of 0.05 nM [^{125}I]BF-180, 100 μl of 100 nM Aβ1–42, and 800 μl of 8% ethanol was incubated at room temperature for 4 h. The mixture was then filtered, and filters containing bound ^{125}I ligand were counted using the γ-counter. Values for half-maximal inhibitory concentration (IC_{50}) were determined from displacement curves of three independent experiments using GraphPad Prism software (GraphPad Software, San Diego, CA), and those for the inhibition constant (K_i) were determined using the Cheng–Prusoff equation.

In addition, fluorescence assay of the compounds with Aβ1–42 and tau fibrils was performed. The 412 aa isoform of human tau was expressed from cDNA clone htau46 in *Escherichia coli* and purified as described previously (Hasegawa et al., 1998). Aβ1–42 (0.2 mg/ml; Peptide Institute) in 50 mM potassium phosphate buffer, pH 7.4, was incubated at 37°C for 72 h with gentle shaking. Tau protein (1 mg/ml) was incubated in the presence of 0.1 mg/ml heparin for 72 h with continuous shaking. Fluorescence spectra of a mixture of the same amount of 0.2 mg/ml Aβ1–42 or 0.1 mg/ml tau and 10, 3, 1, 0.3, 0.1, 0.03, and 0.01 μM concentrations of each compound were measured using a microplate spectrofluorometer (Gemini XS; Molecular Devices, Sunnyvale, CA). Optimal excitation wavelength for the mixture of four BF compounds and Aβ1–42 or tau fibrils were determined. Then, EC_{50} values (effective concentrations to achieve 50% maximal fluorescence intensity at optimal excitation wavelength) were calculated using GraphPad Prism. All measurements were performed in duplicate.

Measurement of octanol/water partition coefficients. 1-Octanol (Wako Pure Chemicals, Osaka, Japan) and PBS was saturated with PBS and 1-octanol before use, respectively. Test compounds were dissolved in 1-octanol and shaken with equal amounts of PBS for 30 min at room temperature. After centrifugation at 2000 per min for 15 min, the absorbency of 1-octanol layer was measured at the peak wavelength of the absorbance spectrum of each compound using a microplate reader (Molecular Devices Spectra Max 190). The octanol/water partition coefficients were determined by comparing the absorbency with that before shaking with PBS. Each data point was performed in duplicate.

Neuropathological staining. Stainability of tested compounds were examined using postmortem brain tissues from cases of autopsy-confirmed AD (78-year-old woman), Pick's disease (75-year-old woman), and progressive supranuclear palsy (PSP) (78-year-old man). Brain sections were obtained from Fukushimura Hospital. Experiments were performed in accordance with the regulations of the ethics committee of the BF Research Institute. Serial sections (6 μm thick) from paraffin-embedded blocks of hippocampus were used for staining. After deparaffinization, quenching of autofluorescence was performed as described previously (Okamura et al., 2004a). Quenched tissue sections were immersed in 100 μM compound or 0.125% thioflavin-S solution containing 50% ethanol for 10 min. Finally, sections were dipped briefly into water, rinsed in PBS for 60 min, coverslipped with FluorSave Reagent (Calbiochem, Darmstadt, Germany), and examined using a Nikon (Tokyo, Japan) Eclipse microscope equipped with a violet filter (excitation, 380–420 nm; dichroic mirror, 430 nm; barrier filter, 450 nm) and a blue filter (excitation, 450–490 nm; dichroic mirror, 505 nm; barrier filter, 520 nm). For the comparison of stainability between BF compounds and thioflavin-S, a blue–violet filter (excitation, 400–440 nm; dichroic mirror, 455 nm; long-pass filter, 470 nm) was used. Staining was also performed in AD brain sections pretreated with 90% formic acid for 5 min. Sections stained with BF compounds were subsequently immunostained with AT8 anti-tau antibody (diluted 1:20; Innogenetics, Ghent, Belgium) to detect tau pathology. An adjacent section was also immunostained with 6F/3D anti-Aβ antibody (diluted 1:50; Dako, High Wycombe, UK). Sections were placed in blocking buffer for 30 min and then incubated at 4°C with primary antibodies for 18 h (AT8) or 1 h (6F/3D). After washing, sections were incubated with biotinylated anti-mouse IgG (Wako Pure Chemicals, Tokyo, Japan) for 60 min, followed by Texas Red-conjugated avidin (Vector Laboratories, Burlingame, CA) for 60 min. After coverslipping, sections were examined using a Nikon Eclipse microscope with a green filter set (excitation, 510–560 nm; dichroic mirror, 575 nm; barrier filter, 590 nm).

In vitro *autoradiography.* A 6-μm-thick section from paraffin-embedded blocks of hippocampus was used for autoradiographic study. After deparaffinization, the section was labeled using 4.7 MBq/ml of [^{11}C]BF-158 at room temperature for 10 min, and then washed briefly with H_2O and 50% ethanol. After drying, the labeled section was exposed to a BAS-III imaging plate (Fujifilm, Tokyo, Japan) for 1 h. Autoradiographic images were obtained using a BAS-5000 phosphorimaging instrument (Fujifilm). Adjacent brain sections were immunostained with anti-tau antibody (AT8) and anti-Aβ antibody (6F/3D), as described previously (Okamura et al., 2004a).

Results

We investigated whether tested compounds would enter the brain in amounts sufficient for *in vivo* brain imaging using PET (Table 1, Fig. 1*C*). The octanol/water partition coefficients of BF-126, BF-158, BF-168, and BF-170 were 12.5, 47.4, 62.6, and 70.3, respectively. These values indicate that these compounds were highly lipophilic. High uptake of these compounds was ap-

Table 1. Octanol/water partition coefficients, brain uptakes at 2 and 30 min after injection in normal mice, K_i values for Aβ 1–42 fibrils, EC_{50} values for Aβ 1–42, and tau fibrils from fluorescence assay of the compounds

	Octanol/water partition coefficient	Brain uptakes (%ID/g)		K_i values for Aβ fibrils (nM)	Fluorescence assay	
		2 min	30 min		EC_{50} for Aβ fibrils (nM)	EC_{50} for τ fibrils (nM)
BF-126	12.5	7.2 ± 0.49	0.16 ± 0.030	1.2 ± 0.68	1280 ± 1.64	583 ± 2.07
BF-158	47.4	11.3 ± 0.81	3.1 ± 0.61	>5000	659 ± 2.04	399 ± 2.41
BF-170	70.3	9.1 ± 1.2	0.25 ± 0.027	>5000	786 ± 1.79	221 ± 2.31
BF-168	62.6	3.9 ± 0.22[a]	1.6 ± 0.0071[a]	6.4 ± 1.0[a]	346 ± 2.21	1010 ± 1.72

Brain uptake and EC_{50} values are shown as the mean ± SEM. K_i values for Aβ fibrils are shown as the mean ± SD.
[a]From Okamura et al., 2004a.

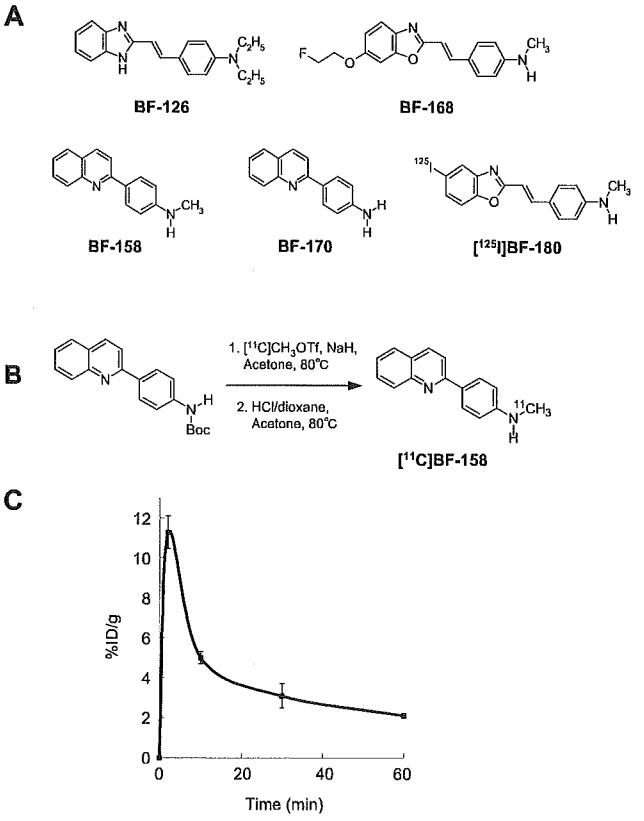

Figure 1. *A*, Chemical structures of BF-126, BF-158, BF-168, BF-170, and [^{125}I]BF-180. *B*, Radiolabeling of BF-158. *C*, The %ID/g obtained in the brains of mice after intravenous administration of [^{11}C]BF-158.

parent in the brain after intravenous administration of each compound, with 7.2%ID/g for BF-126 and 9.1%ID/g for BF-170 at 2 min. These values were higher than those reported previously for compound BF-168 (Okamura et al., 2004a). In addition, brain uptake at 30 min after injection was 0.16%ID/g for BF-126 and 0.25%ID/g for BF-170. Brain uptake of BF-158 was measured using ^{11}C-labeled compound. Brain uptake at 2, 10, 30, and 60 min after intravenous injection of [^{11}C]BF-158 was 11.3 ± 0.81, 5.0 ± 0.31, 3.1 ± 0.61, and 2.1 ± 0.097%ID/g, respectively (Fig. 1*C*). *In vitro* binding of tested compounds to Aβ was examined using synthetic Aβ fibrils. In competitive binding assays with ^{125}I-labeled styrylbenzoxazole compound BF-180, BF-126 displayed high binding affinity to Aβ1–42 fibrils, comparable with BF-168. In contrast, K_i for BF-158 and BF-170 was >5000 nM, suggesting a difference in binding sites between quinoline derivatives and benzoxazole derivatives (Table 1). In the fluorescence binding assay of the mixture of tested compounds and Aβ1–42 fibrils, EC_{50} value was lowest in BF-168, suggesting higher affinity to Aβ compared with the other agents. In contrast, in the assay of the mixture of compounds with tau fibrils, EC_{50} values of BF-170, BF-158, and BF-126 was lower than that of BF-168, suggesting relatively higher binding affinity to tau fibrils.

Subsequently, neuropathological staining was performed using AD brain samples to examine the *in vitro* binding characteristics of tested compounds for AD pathology. BF-126, BF-158, and BF-170 clearly stained NFTs and neuropil threads in the hippocampal section of AD brain (Fig. 2*A–C*). In the comparison with tau immunostaining in the same sections, binding of these compounds with tau pathology was confirmed. In contrast, SPs were faintly stained with BF-126, BF-158, and BF-170, as opposed to clear staining of SPs with thioflavin-S (Fig. 2*A–C*). We further investigated the stainability of neuritic changes using these compounds and BF-168. BF-168 clearly visualized both the central core and peripheral zone of core plaques under violet and blue filters (Fig. 2*D*). The staining pattern for BF-168 did not coincide with that for tau immunostaining in the same section but closely resembled Aβ immunostaining in the adjacent section (Fig. 2*D*). In contrast, BF-126, BF-158, and BF-170 predominantly stained neuritic elements under a blue filter and coincided well with tau immunostaining (Fig. 2*E–G*). Under a violet filter, the central core and peripheral halo were barely visible. These findings suggest that BF-126, BF-158, and BF-170 prefer to bind to PHF-type neurites rather than Aβ fibrils. Pretreatment with formic acid eliminated the staining of NFTs with BF-170 (Fig. 2*H, I*), BF-158, and BF-126 (data not shown), suggesting that both compounds recognize the β-sheet structure of NFTs rather than monomeric tau protein. To investigate whether these compounds detect neuropathological lesions in non-AD tauopathy, staining was performed in brain sections from Pick's disease and PSP patients. As a result, BF-126, BF-170, and BF-158 (data not shown) were unable to identify Pick bodies (Fig. 2*J*), globose tangles (Fig. 2*K*), and glial pathology in PSP brain (data not shown).

Finally, *in vitro* autoradiography using [^{11}C]BF-158 was performed in AD brain section. Accumulation of tracer was observed primarily in the gray matter region of the brain. The distribution of labeling with [^{11}C]BF-158 correlated well with tau immunostaining in the adjacent section (Fig. 3*A, B*). In particular, high levels of tracer accumulation were observed in NFT-rich brain regions (Fig. 3*D, E*, arrows). This finding indicates the binding of [^{11}C]BF-158 for NFTs in the AD brain.

Discussion

Although the present research did not confirm whether the studied compounds can visualize tau pathology in the living brain, the results strongly suggest that quinoline and benzimidazole derivatives represent potential candidates for an *in vivo* tau-imaging agent in AD patients. Requirements for the ideal tau-imaging probe include the following: (1) high BBB and cell membrane permeability; (2) rapid clearance from normal brain tissue; (3) high affinity for NFTs, neuropil threads, and PHF-type neurites; and (4) low nonspecific binding. Our results indicate that BF-126, BF-158, and BF-170 display sufficient BBB permeability for use as PET imaging tracers. Permeability of the neuronal membrane represents another important factor for *in vivo* imaging of intracellular tau aggregates (Small et al., 2002). High lipophilicity

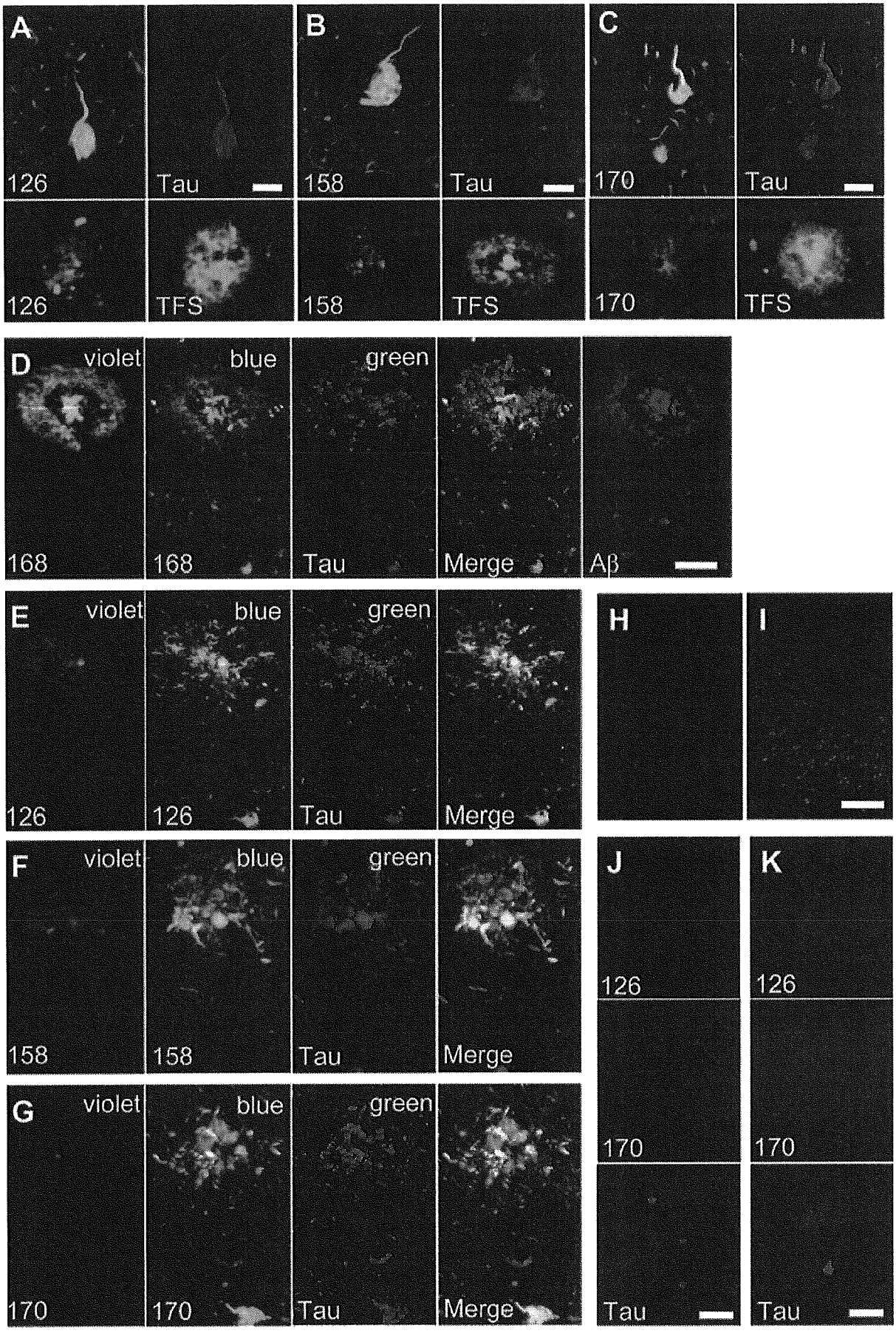
A
126
Tau
126
TFS
B
158
Tau
158
TFS
C
170
Tau
170
TFS
D
violet
blue
green
168
168
Tau
Merge
Aβ
E
violet
blue
green
126
126
Tau
Merge
F
violet
blue
green
158
158
Tau
Merge
G
violet
blue
green
170
170
Tau
Merge
H
I
J
126
170
Tau
K
126
170
Tau

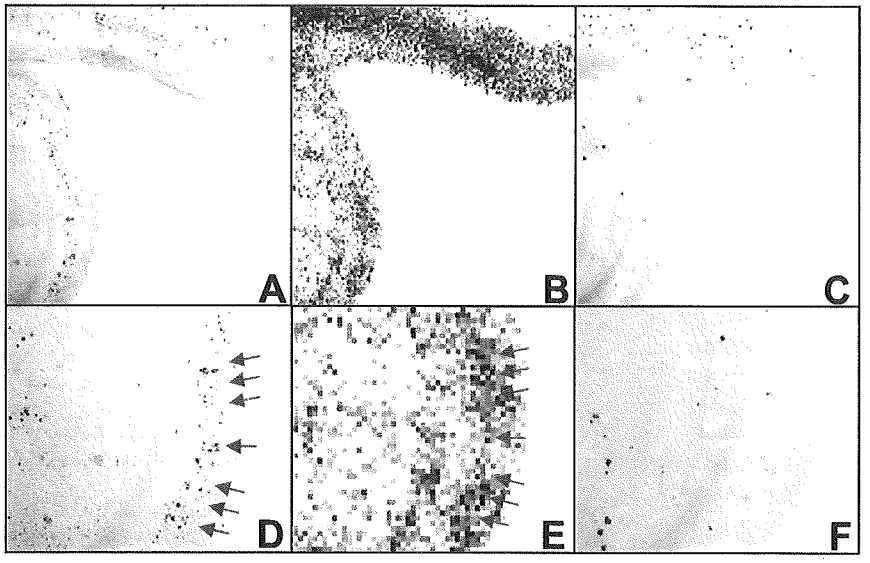

Figure 3. ***A–C***, Autoradiography of AD hippocampal brain section using [^{11}C]BF-158 (***B***) and immunostaining by anti-tau (***A***) and anti-Aβ (***C***) antibodies in adjacent sections. ***D–F***, Close-up images of ***A***, ***B***, and ***C***, respectively. ***D***, ***E***, Accumulation of [^{11}C]BF-158 (***E***, arrows) correlates well with tau immunostaining (***D***).

of these compounds has the advantage in this factor. *In vivo* imaging using a tangle-laden mouse model that accurately reflects AD pathology will elucidate this issue. Furthermore, three tested compounds demonstrated fast clearance from normal brain tissue. This property will contribute to improving the sensitivity of detecting NFT accumulation by minimizing residual background levels of tracer.

The most intriguing point of this study was that BF-126, BF-158, and BF-170 have a preference for tau pathology in AD brain. Results from fluorescence binding assay suggest relatively higher binding affinity to tau fibrils of these three compounds. These compounds also show excellent stainability for tau pathology and little background fluorescence in AD brain. An autoradiographic study using [^{11}C]BF-158 confirmed the accumulation of this tracer in tangle-rich brain regions, emphasizing the binding preference of these compounds to tau pathology in AD brains. However, fluorescence assay data show the binding ability of these agents to Aβ fibrils. In neuropathological staining, these agents faintly stained amyloid plaques. Thus, these compounds are not completely specific to tau pathology. Nevertheless, our data suggest that these three agents have relatively higher binding affinity to tau pathology rather than to Aβ pathology in AD brain.

Previous neuropathological research suggests that the deposition of NFTs occurs before the presentation of clinical symptom in AD. Even in the very early stages of AD, patients display considerable numbers of NFTs in the entorhinal cortex and hippocampus, sufficient for the neuropathological diagnosis of AD. Thus, *in vivo* imaging of NFTs in conjunction with imaging SPs could prove useful for the early and accurate diagnosis of AD. Quantitative evaluation of tau pathology could also be helpful for tracking severity of dementia, because the formation of neuritic pathology correlates well with clinical severity of dementia (Dickson, 1997). NFT deposition in the entorhinal cortex is closely associated with neuronal loss in very early AD patients (Gomez-Isla et al., 1996). Prevention of NFT formation is thus an important target of anti-dementia drugs. If novel treatments that prevent the pathological formation of neurofibrillary pathology could be turned into clinical applications, this imaging technique would be applicable for the evaluation of treatment efficacy.

The general mechanism of abnormal protein aggregation leading to disease is β-sheet formation. AD is accompanied by the formation of two distinct β-sheet aggregates, Aβ fibrils and PHFs. As is the case with previously reported imaging agents, BF-126, BF-158, and BF-170 recognize β-pleated sheet structure, because staining in AD brain sections was disturbed by pretreatment with formic acid (Kitamoto et al., 1987). Our results suggest that tested compounds display relatively higher binding affinities to PHFs than to Aβ fibrils. Previous reports describe 2-(1-{6-[(2-fluoroethyl)(methyl)amino]-2-naphthyl}ethylidene)malononitrile (FDDNP) as a candidate of tau imaging agent (Agdeppa et al., 2001). This compound is a highly lipophilic agent and specifically labels NFTs as well as SPs in AD brain sections. [^{18}F]FDDNP, the first PET probe to see clinical use for AD patients, reportedly detects the combined signals of SPs and NFTs (Shoghi-Jadid et al., 2002). FDDNP shows high binding affinity to Aβ fibrils; however, binding affinity to tau fibrils is unknown. Pittsburgh compound B, another promising PET probe, preferentially detects the accumulation of SPs rather than NFTs (Klunk et al., 2003). BF-145 and TZDM (2-[4′-(dimethylamino)phenyl]-6-iodobenzothiazole) also reportedly preferentially recognize SPs (Kung et al., 2003; Okamura et al., 2004b). Why these β-sheet binding agents show such a variety of binding characteristics with SPs and NFTs is not well understood. The diameter of a PHF is 18–20 nm at the widest portion and 8–10 nm at the narrowest portion (Wisniewski et al., 1984), whereas Aβ fibrils are 7–12 nm in diameter (Sunde et al., 1997). Although the nature of PHF structure remains contentious, both structures share a common pattern, with 4.76 Å meridional spacing and 10.6 Å equatorial spacing, characteristic of a cross-β structure (Berriman et al., 2003; Balghorn et al., 2004). A recent study indicated the presence of multiple ligand-binding sites on Aβ fibrils (Lockhart et al., 2005). If

←

Figure 2. ***A–J***, Neuropathological staining of brain sections from cases of AD (***A–I***), Pick's disease (***J***), and progressive supranuclear palsy (***K***). BF-126 (***A***), BF-158 (***B***), and BF-170 (***C***) clearly stained neurofibrillary tangles and neuropil threads. These stainings were consistent with tau immunostaining. In contrast, these compounds faintly stained amyloid plaques, which were clearly stained with thioflavin-S (TFS) in adjacent sections. ***D–G***, Double staining with BF compounds and anti-tau antibody was performed in hippocampal brain sections. ***D***, Cored plaque is clearly visualized by BF-168 using violet and blue filters. A merged image of BF-168 fluorescence using a blue filter and tau immunostaining (green) indicates that BF-168 does not recognize PHF-type neurites. The image of Aβ immunostaining in an adjacent section closely resembles BF-168 staining. BF-126 (***E***), BF-158 (***F***), and BF-170 (***G***) faintly stain the core and halo of amyloid plaque using a violet filter. However, images using a blue filter closely resemble tau immunostaining. ***E–I***, A merged image indicates that these three compounds preferentially bind to PHF-type neurites (***E–G***). BF-170 (***H***), BF-158, and BF-126 (data not shown) did not stain any pathological structures in the section pretreated with formic acid, in contrast to the clear visualization of NFTs in non-pretreated brain sections (***I***). ***J***, ***K***, Staining of Pick bodies and globose tangles were compared with tau immunostaining in brain sections from cases of Pick's disease (***J***) and progressive supranuclear palsy (***K***). Neither Pick bodies (***G***; green) nor globose tangles (***H***; green) are detected in brain sections treated with BF-126 and BF-170. Scale bars: ***A–C***, 25 μm; ***D–G***, 50 μm; ***H–I***, 400 μm; ***J–K***, 100 μm

PHF also includes multiple binding sites for β-sheet binding agents, this factor will contribute to the difference in ligand-binding affinity to SPs and NFTs. The manner of binding between β-sheet binding agents and both NFTs and SPs is not well clarified. However, differences in conformation between SPs and NFTs and differences in ligand-binding sites may result in the diversity of binding properties in these compounds to SPs and NFTs.

Tau lesions are not only the hallmark of AD but are also characteristic of non-AD tauopathy such as PiD and PSP (Goedert, 2004). However, tested compounds did not show any significant binding to pathological lesions in these diseases, implying that both compounds are highly specific to PHFs in AD. Accordingly, these probes are potentially useful for differentiating between AD and other neurodegenerative disorders. For future clinical applications, optimization of the compounds is necessary to assure compound safety, facilitate radiolabeling, and reduce nonspecific binding. We are currently investigating the *in vivo* binding characteristics of these optimized probes.

References

Agdeppa ED, Kepe V, Liu J, Flores-Torres S, Satyamurthy N, Petric A, Cole GM, Small GW, Huang SC, Barrio JR (2001) Binding characteristics of radiofluorinated 6-dialkylamino-2-naphthylethylidene derivatives as positron emission tomography imaging probes for β-amyloid plaques in Alzheimer's disease. J Neurosci 21:RC189(1–5).

Barghorn S, Davies P, Mandelkow E (2004) Tau paired helical filaments from Alzheimer's disease brain and assembled in vitro are based on beta-structure in the core domain. Biochemistry 43:1694–1703.

Berriman J, Serpell LC, Oberg KA, Fink AL, Goedert M, Crowther RA (2003) Tau filaments from human brain and from in vitro assembly of recombinant protein show cross-beta structure. Proc Natl Acad Sci USA 100:9034–9038.

Braak H, Braak E (1991) Neuropathological stageing of Alzheimer-related changes. Acta Neuropathol (Berl) 82:239–259.

Dickson DW (1997) Neuropathological diagnosis of Alzheimer's disease: a perspective from longitudinal clinicopathological studies. Neurobiol Aging 18 [4 Suppl]:S21–S26.

Goedert M (2004) Tau protein and neurodegeneration. Semin Cell Dev Biol 15:45–49.

Gomez-Isla T, Price JL, McKeel Jr DW, Morris JC, Growdon JH, Hyman BT (1996) Profound loss of layer II entorhinal cortex neurons occurs in very mild Alzheimer's disease. J Neurosci 16:4491–4500.

Hasegawa M, Smith MJ, Goedert M (1998) Tau proteins with FTDP-17 mutations have a reduced ability to promote microtubule assembly. FEBS Lett 437:207–210.

Kitamoto T, Ogomori K, Tateishi J, Prusiner SB (1987) Formic acid pretreatment enhances immunostaining of cerebral and systemic amyloids. Lab Invest 57:230–236.

Klunk WE, Wang Y, Huang GF, Debnath ML, Holt DP, Shao L, Hamilton RL, Ikonomovic MD, DeKosky ST, Mathis CA (2003) The binding of 2-(4′-methylaminophenyl)benzothiazole to postmortem brain homogenates is dominated by the amyloid component. J Neurosci 23:2086–2092.

Klunk WE, Engler H, Nordberg A, Wang Y, Blomqvist G, Holt DP, Bergstrom M, Savitcheva I, Huang GF, Estrada S, Ausen B, Debnath ML, Barletta J, Price JC, Sandell J, Lopresti BJ, Wall A, Koivisto P, Antoni G, Mathis CA, et al. (2004) Imaging brain amyloid in Alzheimer's disease with Pittsburgh Compound-B. Ann Neurol 55:306–319.

Kung MP, Skovronsky DM, Hou C, Zhuang ZP, Gur TL, Zhang B, Trojanowski JQ, Lee VM, Kung HF (2003) Detection of amyloid plaques by radioligands for Aβ40 and Aβ42: potential imaging agents in Alzheimer's patients. J Mol Neurosci 20:15–24.

Kung MP, Hou C, Zhuang ZP, Skovronsky D, Kung HF (2004) Binding of two potential imaging agents targeting amyloid plaques in postmortem brain tissues of patients with Alzheimer's disease. Brain Res 1025:98–105.

Lee VM, Balin BJ, Otvos Jr L, Trojanowski JQ (1991) A68: a major subunit of paired helical filaments and derivatized forms of normal tau. Science 251:675–678.

Lockhart A, Ye L, Judd DB, Merritt AT, Lowe PN, Morgenstern JL, Hong G, Gee AD, Brown J (2005) Evidence for the presence of three distinct binding sites for the thioflavin T class of Alzheimer's disease PET imaging agents on beta-amyloid peptide fibrils. J Biol Chem 280:7677–7684.

Mathis CA, Wang Y, Klunk WE (2004) Imaging beta-amyloid plaques and neurofibrillary tangles in the aging human brain. Curr Pharm Des 10:1469–1492.

Nordberg A (2004) PET imaging of amyloid in Alzheimer's disease. Lancet Neurol 3:519–527.

Okamura N, Suemoto T, Shimadzu H, Suzuki M, Shiomitsu T, Akatsu H, Yamamoto T, Staufenbiel M, Yanai K, Arai H, Sasaki H, Kudo Y, Sawada T (2004a) Styrylbenzoxazole derivatives for *in vivo* imaging of amyloid plaques in the brain. J Neurosci 24:2535–2541.

Okamura N, Suemoto T, Shiomitsu T, Suzuki M, Shimadzu H, Akatsu H, Yamamoto T, Arai H, Sasaki H, Yanai K, Staufenbiel M, Kudo Y, Sawada T (2004b) A novel imaging probe for in vivo detection of neuritic and diffuse amyloid plaques in the brain. J Mol Neurosci 24:247–255.

Price JL, Morris JC (1999) Tangles and plaques in nondemented aging and "preclinical" Alzheimer's disease. Ann Neurol 45:358–368.

Shoghi-Jadid K, Small GW, Agdeppa ED, Kepe V, Ercoli LM, Siddarth P, Read S, Satyamurthy N, Petric A, Huang SC, Barrio JR (2002) Localization of neurofibrillary tangles and beta-amyloid plaques in the brains of living patients with Alzheimer disease. Am J Geriatr Psychiatry 10:24–35.

Small GW, Agdeppa ED, Kepe V, Satyamurthy N, Huang SC, Barrio JR (2002) In vivo brain imaging of tangle burden in humans. J Mol Neurosci 19:323–327.

Sunde M, Serpell LC, Bartlam M, Fraser PE, Pepys MB, Blake CC (1997) Common core structure of amyloid fibrils by synchrotron X-ray diffraction. J Mol Biol 273:729–739.

Wisniewski HM, Merz PA, Iqbal K (1984) Ultrastructure of paired helical filaments of Alzheimer's neurofibrillary tangle. J Neuropathol Exp Neurol 43:643–656.

Journal of Infection (2005) 50, 394-396

ELSEVIER

BRITISH INFECTION SOCIETY

www.elsevierhealth.com/journals/jinf

Cerebroventricular infusion of pentosan polysulphate in human variant Creutzfeldt-Jakob disease

N.V. Todd[a], J. Morrow[b], K. Doh-ura[c], S. Dealler[d], S. O'Hare[e], P. Farling[f], M. Duddy[b], N.G. Rainov[g,*]

[a]*Regional Neurosciences Centre, Newcastle General Hospital NHS Trust, Newcastle, UK*
[b]*Department of Neurology, Royal Victoria Hospital, Belfast, UK*
[c]*Department of Prion Research, Tohoku University Graduate School of Medicine, Japan*
[d]*Department of Microbiology, Lancaster General Infirmary; Lancaster, UK*
[e]*Department of Pharmacy, Royal Victoria Hospital, Belfast, UK*
[f]*Department of Anesthetics, Royal Victoria Hospital, Belfast, UK*
[g]*Department of Neurological Science, The University of Liverpool, and The Walton Centre for Neurology and Neurosurgery NHS Trust, Lower Lane, Liverpool L9 7LJ, UK*

Accepted 24 July 2004
Available online 22 September 2004

KEYWORDS
Brain;
Intraventricular;
New variant CJD;
Pentosan polysulphate

Abstract Variant Creutzfeldt-Jakob disease (CJD) is a transmissible spongiform encephalopathy believed to be caused by the bovine spongiform encephalopathy agent, an abnormal isoform of the prion protein (PrP^{sc}). At present there is no specific or effective treatment available for any form of CJD. Pentosan polysulphate (PPS), a large polyglycoside molecule with weak heparin-like activity, has been shown to prolong the incubation period of the intracerebral infection when administered to the cerebral ventricles in a rodent scrapie model. PPS also prevents the production of further PrP^{sc} in cell culture models.

These properties of PPS prompted its cerebroventricular administration in a young man with vCJD. Long-term continuous infusion of PPS at a dose of 11 μg/kg/day for 18 months did not cause drug-related side effects. Follow-up CT scans demonstrated progressive brain atrophy during PPS administration. Further basic and clinical research is needed in order to address the issue of efficacy of PPS in vCJD and in other prion diseases.

Introduction

Variant Creutzfeldt-Jakob disease (vCJD) is a form of CJD believed to be caused by the bovine spongiform encephalopathy agent.[1-3] Unlike the

* Corresponding author. Tel.: +44-151-529-5323; fax: +44-151-529-5465.
E-mail address: rainov@liv.ac.uk (N.G. Rainov).

0163-4453/$30.00
doi:10.1016/j.jinf.2004.07.015

sporadic form, vCJD mostly becomes symptomatic in young adults and adolescents.[1] Pentosan polysulphate (PPS) is a large polyglycoside molecule with weak heparin-like activity. It has been shown to prevent the propagation of the abnormal isoform of the prion protein (PrP^{sc}) in cell culture models,[4] and to prolong the incubation period of intracerebral infection in rodent scrapie models when administered either systemically[5] or directly into the cerebral ventricles.[6] These properties of PPS prompted our use of cerebroventricular PPS in escalating doses in one patient with vCJD to assess the safety and tolerability of the drug when administered by this route.

Case report and discussion

The patient is a 20-year-old man who presented initially at the age of 16 years and 11 months with subjective signs of behavioural disturbance. A few months later this was followed by progressive ataxia, pyramidal signs and myoclonus, which led to the clinical diagnosis of possible vCJD. The clinical picture combined with abnormal MR findings in the FLAIR sequence (pulvinar sign) and positive tonsil biopsy allowed the diagnosis of probable vCJD 8 months after the initial clinical symptoms (Fig. 1). At the time of initial administration of PPS (Pentosan polysulphate SP54, Bene Arzneimittel GmbH, Munich, Germany) into the cerebral ventricular system, the patient had symptoms of advanced vCJD,[7] such as ataxia, dementia, dysphagia, dysphasia, myoclonus, and was confined to bed and unable to care for himself. He was fed via percutaneous gastrostomy.

A permanently implanted right frontal intraventricular catheter was connected to a subcutaneous programmable pump (Synchromed EL, Medtronic Inc.). The initial PPS dose of 1 μg/kg/d was escalated without significant problem to the target dose, extrapolated from animal studies, of 11 μg/kg/d. A possible therapeutic dose-effect relationship for intracerebroventricular PPS in humans with prion disease remains unknown, and therefore further dose escalation would only be limited by side effects. In mice, dose-response studies with PPS have shown that the most effective dose is 230 μg/kg/d.[6] In our current human dosing this would translate to 23 μg/kg/d, which is a little more than twice the current daily dose of PPS.

Continuous infusion of PPS for 18 months did not cause any drug-related side effects. Cerebroventricular PPS at the above dose did not have any measurable systemic anticoagulant activity in serum, as confirmed by unchanged INR (international normalised ratio) before and during PPS infusion.

Follow-up CT scans demonstrated no intracerebral haemorrhage (Fig. 2), and there were no seizures. A right parietal subdural fluid collection of increasing size was noted on CT scans 8 months after start of PPS infusion and necessitated surgical (burr hole) evacuation of fluid. PPS infusion was halted temporarily and restarted one week after the surgery. Due to recurrent subdural fluid collections, two further surgical revisions were necessary.

Clearly comments on efficacy are difficult in the setting of a single case, but after 18 months of continuous cerebroventricular PPS administration, the patient is still alive and there is some evidence of a change in the neurological condition. He is now able to fix his eyes on persons, to obey simple one stage commands, and to make verbalization attempts in response to stimuli. The sleep/wake cycle and the reflex swallow are restored and the

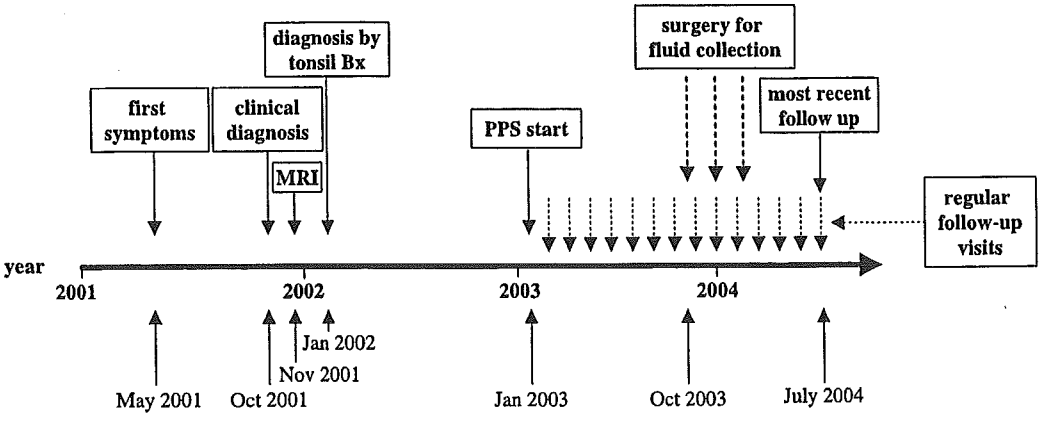

Figure 1 Schematic representation of the time course of disease presentation, diagnosis and management. Bx= biopsy.

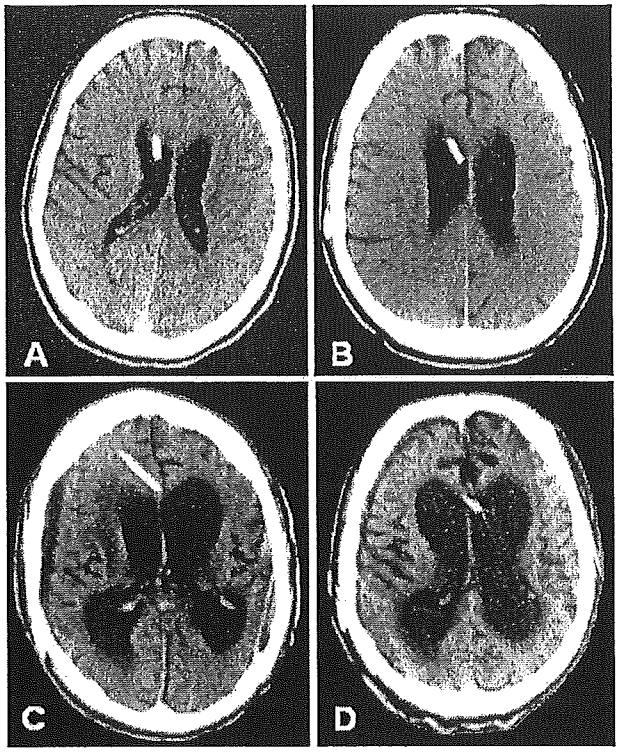

Figure 2 (A) Non-enhanced CT scan on day 6 after start of cerebroventricular PPS infusion. (B) Non-enhanced CT scan 3 months after start of PPS infusion. Note the slightly enlarged lateral ventricles compared to baseline (A). (C) Non-enhanced CT scan 1-year after start of PPS infusion. (D) Non-enhanced CT scan 15 months after start of PPS infusion. Note progressing cortical and subcortical atrophy with enlargement of the ventricular system on scans C and D.

myoclonus is reduced. The patient has gained 5 kg of weight compared to pre-PPS baseline, while on the same nutritional regime. Regular follow-up observations and pump refills (every 6 weeks) were carried out by the same medical and nursing staff and physiotherapists involved with the patient's care from the early stages of his disease. Despite the apparent trend towards clinical improvement, brain atrophy, as seen on regular follow-up CT scans, continued to progress during the period of PPS administration and resulted in ventriculomegaly and grossly enlarged extracerebral CSF spaces (Fig. 2).

In conclusion, cerebroventricular infusion of PPS at 11 μg/kg/d appears safe and well tolerated for continuous long-term application. Our patient has survived for 37 months after initial symptoms and 30 months after diagnosis of probable vCJD, while the median duration of illness with vCJD is 13 months (range 6-39)[7].

Further lessons have also been learned from this first case. Firstly, surgery in a brain affected by vCJD may result in a higher rate of surgical complications than might be expected in a normal patient. We suggest that in order to allow the catheter track to organise, drug infusion should be delayed for at least 7-10 days after implantation of the pump system. Regular neuroradiological follow-up throughout the treatment period is strongly recommended. Secondly, if clinically significant benefits are to be expected, PPS administration should start as early as possible in the course of the disease and before irreversible loss of neurological function has occurred.

Further clinical, neuroradiological and laboratory investigations in the setting of a prospective clinical study with standardised follow-up protocol and data collection are essential in order to assess the efficacy of PPS administration in vCJD and in other prion diseases.

Acknowledgements

The authors would like to thank Dr R. Knight (Edinburgh) and Dr C. Pomfrett (Manchester) for useful comments and suggestions regarding the manuscript. Dr M. McClean (Belfast) is gratefully acknowledged for his general medical input and practical support.

References

1. Will RG, Ironside JW, Zeidler M, Cousens SN, Estibeiro K, Alperovitch A, Poser S, Pocchiari M, Hofman A, Smith PG. A new variant of Creutzfeldt-Jakob disease in the UK. *Lancet* 1996;**347**:921-5.
2. Bruce ME, Will RG, Ironside JW, McConnell I, Drummond D, Suttie A, McCardle L, Chree A, Hope J, Birkett C, Cousens S, Fraser H, Bostock CJ. Transmissions to mice indicate that 'new variant' CJD is caused by the BSE agent. *Nature* 1997; **389**:498-501.
3. Hill AF, Desbruslais M, Joiner S, Sidle KC, Gowland I, Collinge J, Doey LJ, Lantos P. The same prion strain causes vCJD and BSE. *Nature* 1997;**389**:448-50.
4. Caughey B, Raymond GJ. Sulfated polyanion inhibition of scrapie-associated PrP accumulation in cultured cells. *J Virol* 1993;**67**:643-50.
5. Ladogana A, Casaccia P, Ingrosso L, Cibati M, Salvatore M, Xi YG, Masullo C, Pocchiari M. Sulphate polyanions prolong the incubation period of scrapie infected hamsters. *J Gen Virol* 1992;**73**:661-5.
6. Doh-ura K, Ishikawa K, Murakami-Kubo I, Sasaki K, Mohri S, Race R, Iwaki T. Treatment of transmissible spongiform encephalopathy by intraventricular drug infusion in animal models. *J Virol* 2004;**78**:4999-5006.
7. Henry C, Knight R. Clinical features of variant Creutzfeldt-Jakob disease. *Rev Med Virol* 2002;**12**:143-50.

ELSEVIER

Journal of the Neurological Sciences 232 (2005) 45–49

Journal of the Neurological Sciences

www.elsevier.com/locate/jns

Diffusion-weighted MRI in familial Creutzfeldt–Jakob disease with the codon 200 mutation in the prion protein gene

Yoshio Tsuboi[a,*], Yasuhiko Baba[b], Katsumi Doh-ura[c], Akiko Imamura[a], Shinsuke Fujioka[a], Tatsuo Yamada[a]

[a]*Fifth Department of Internal Medicine, Fukuoka University School of Medicine, 7-45-1 Nanakuma, Johnan-ku, Fukuoka 814-0180, Japan*
[b]*Department of Neurology, Mayo Clinic Jacksonville, Florida, USA*
[c]*Department of Prion Research, Tohoku University, Sendai, Japan*

Received 28 July 2004; received in revised form 11 January 2005; accepted 12 January 2005
Available online 25 February 2005

Abstract

Magnetic resonance imaging (MRI) with diffusion-weighted imaging (DWI) has been reported to be a useful tool for early diagnosis of sporadic Creutzfeldt–Jakob disease (CJD). We report MRI findings with DWI, as well as with fluid-attenuated inversion recovery (FLAIR) and T1-weighted imaging (T1WI), in a case of familial CJD with a mutation at codon 200 of the prion protein gene. DWI in this patient showed high signal intensity in the basal ganglia and the cerebral cortex, similar to findings in sporadic CJD. In addition, T1WI showed areas of high signal intensity bilaterally in the globus pallidus. Despite the clinical diversity and atypical laboratory findings seen in familial CJD with the codon 200 mutation, these neuroimaging studies suggest that common regional distributions and a common pathogenesis might underlie the clinical progression both in sporadic CJD and in familial CJD with the codon 200 mutation in the prion protein gene. DWI abnormalities may be characteristic features that should be considered in the diagnosis of familial as well as of sporadic CJD.

Keywords: Creutzfeldt–Jakob disease; Diagnostic methods; Diffusion-weighted imaging; Familial; Magnetic resonance imaging; Prion disease; Prion gene mutation

1. Introduction

Creutzfeldt–Jakob disease (CJD) is a rare and fatal neurodegenerative disorder caused by abnormal prion protein accumulation in the brain [1–3]. CJD may occur in sporadic, infectious, or familial forms. The familial form is found in 10% to 15% of all cases of CJD [4]. The diagnosis of CJD is usually based on clinical features, characteristic electroencephalographic (EEG) activity, and laboratory values. The clinical features consist of rapidly progressive dementia, myoclonus, and ataxia and are typically fatal within 1 year from the onset of symptoms [1–3]. EEG activity in CJD is characterized by periodic sharp and slow wave complexes [5]. Laboratory criteria include an elevated concentration of neuron-specific enolase (NSE) and the presence of 14–3–3 protein in the cerebrospinal fluid (CSF) [5–8].

Diagnosis of familial CJD is often difficult because clinical presentation varies widely, and characteristic features are not always present [6,9]. Familial CJD can be caused by several different mutations in the prion protein gene [4]. Atypical clinical features may be related to different genotypes at codon 129 or 219 [10,11]. One mutation at codon 200 in the prion protein gene is known to present with diverse clinical characteristics ranging from features similar to those of sporadic CJD [12–15] to atypical features such as slow progression of symptoms, fatal insomnia, polyneuropathy, lack of characteristic EEG

* Corresponding author. Tel.: +81 92 801 1011; fax: +81 92 865 7900.
E-mail address: tsuboi@cis.fukuoka-u.ac.jp (Y. Tsuboi).

0022-510X/$ - see front matter © 2005 Elsevier B.V. All rights reserved.
doi:10.1016/j.jns.2005.01.006

abnormalities, and absence of 14–3–3 protein in the CSF [10,16,17].

Thus, a useful diagnostic tool is needed, particularly for patients without a known family history of CJD. The presence of 14–3–3 protein in the CSF has been recognized to have good sensitivity and specificity as an indicator of sporadic CJD [5–7,18]. However, no studies have been published on the sensitivity and specificity of CSF abnormalities in familial CJD, and as many as 25% of patients with familial CJD may have normal 14–3–3 protein and NSE concentrations in the CSF [5,6].

Magnetic resonance imaging (MRI) has been reported to be a useful tool for early diagnosis of sporadic CJD. For example, MRI with diffusion-weighted images (DWI) shows increased signals in the basal ganglia and cerebral cortex of patients with sporadic CJD [19–28]. Whether MRI is equally useful in the diagnosis of familial CJD remains unclear, although several MRI studies have been reported in familial CJD with various mutations in the prion protein gene [29–32].

To further investigate whether MRI might be useful in the diagnosis of familial CJD, we examined the brain of a patient with familial CJD in whom the codon 200 mutation was confirmed by molecular genetic analysis. DWI, fluid-attenuated inversion recovery (FLAIR) imaging, and T1-weighted imaging (T1WI) were performed, and the results were compared with findings in the literature on patients with sporadic CJD.

2. Case report

2.1. Clinical description

A 64-year-old right-handed woman born in southern Japan was admitted to our hospital because of forgetfulness, dysarthria, and impaired balance. She had noticed the forgetfulness and insomnia 3 months before admission. Fatigue, motor slowness, and dysarthria had developed 2 months before admission. The frequency of spontaneous speech had gradually decreased, and she had increasingly experienced loss of balance, leading to falls. The patient's mother died at age 55 of a progressive dementing disorder, and her younger sister had received a diagnosis of familial CJD at another hospital.

At admission to our hospital, the patient was alert and cooperative, but inattentive. She was able to follow simple commands, and her Mini-Mental State Examination (MMSE) score at that time was 23 of 30 possible points. Her speech was slurred, and scanning speech was occasionally evident. Her pupils were normal in size and reacted to light stimulation. Extraocular movement was normal. Cerebellar ataxia was detected, including dysmetria and decomposition in all extremities. Her gait was also ataxic and wide based. No involuntary movements were observed. She did not smoke or consume alcohol and had no history of toxic exposure. Results of extensive laboratory evaluations of serum, urine, and CSF were normal, except for positive

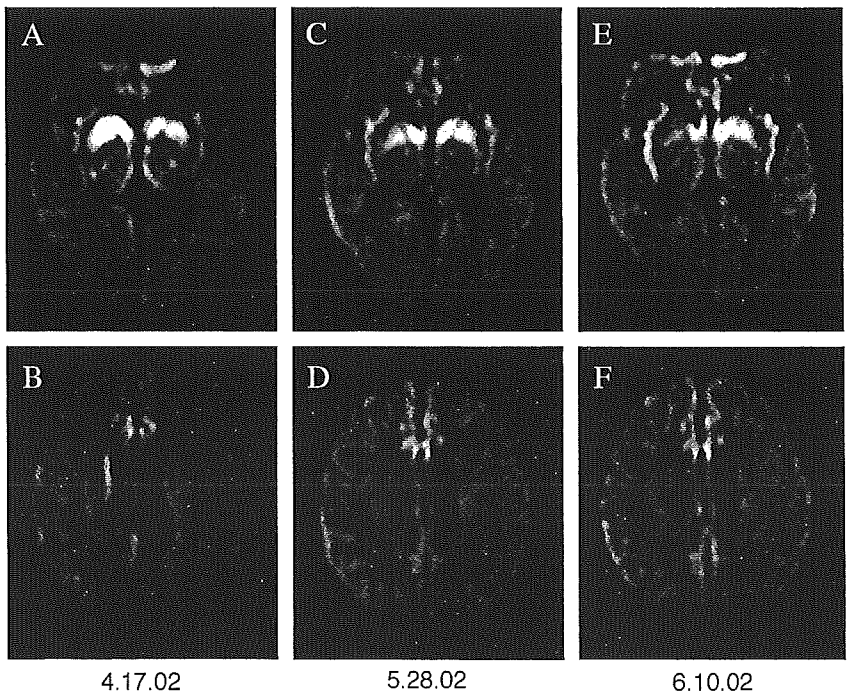

Fig. 1. Magnetic resonance imaging of the brain of a patient with familial Creutzfeldt–Jakob disease, performed with serial diffusion-weighted images (DWI). (A) and (B) were performed at admission to hospital, (C) and (D) at approximately 1 month, and (E) and (F) at 2 months after admission. (A) and (B) High signal intensity bilaterally in the basal ganglia, insula, and cingulate gyrus. (C) and (D) Slightly decreased hyperintense bilateral signals in the basal ganglia; extension of signals in the cortex into left temporoparietal cortex and cingulate gyrus. (C) Increased signal intensity in areas of hyperintensity in insular cortex. (E) and (F) Slight decrease in hyperintense signals in cingulate gyrus, insular cortex, left temporoparietal cortex, and basal ganglia.

14–3–3 protein (+; normal, negative) and elevated NSE (77 ng/mL; normal, <35 ng/mL) in the CSF. At that time, EEG showed diffuse slow waves without periodic sharp waves.

A diagnosis of familial CJD was made, and treatment with quinacrine was started at 300 mg/day. Despite treatment, the patient's speech and gait deteriorated rapidly. Her cognitive decline also progressed rapidly in association with myoclonic jerks in the upper extremities. Subsequently, both spontaneous and stimulus-induced episodes of myoclonus were seen in all extremities. Rigidity, Babinski signs, snout reflex, and bilateral grasping reflex also developed. One month after admission (4 months after the onset of symptoms), EEG showed diffuse slow and periodic sharp-wave complex discharges.

Genomic DNA was extracted from peripheral lymphocytes. The coding sequence of the prion protein gene was amplified by using polymerase chain reaction. Genetic study confirmed the point mutation at codon 200 (GAG→AAG) resulting in the substitution of lysine for glutamate.

2.2. Magnetic resonance imaging studies

MRI of the brain was performed with DWI, FLAIR imaging, and T1WI at admission, as well as approximately 1 and 2 months later.

At admission, DWI demonstrated high signal intensity bilaterally in the basal ganglia, insula, and cingulate gyrus (Fig. 1A and B). FLAIR imaging also showed high signal intensity bilaterally in the basal ganglia (Fig. 2A). Apparent diffusion coefficient (ADC) mapping of these regions revealed decreased signal intensity, indicating cytotoxic edema. T1-weighted imaging (T1WI) showed normal results (Fig. 2B).

DWI performed approximately 1 month after admission showed that the hyperintense signals in the basal ganglia had decreased slightly and those in the cortex had extended into the left temporoparietal cortex and the cingulate gyrus (Fig. 1C and D). DWI also showed that the hyperintensity in the insular cortex had increased in signal intensity (Fig. 1C). On T1WI, spotty hyperintense signals had appeared bilaterally in the globus pallidus (Fig. 2D).

On DWI performed 2 months after admission, the degree of hyperintensity in regions involving the cingulate gyrus, insular cortex, left temporoparietal cortex, and basal ganglia had decreased slightly (Fig. 1E and F). On T1WI, the increased signal intensity in the globus pallidus was more apparent than it had been 1 month after admission (Fig. 2F).

3. Discussion

The case we describe helps to clarify the role of MRI as a diagnostic tool in patients with familial CJD. Familial CJD with the codon 200 mutation was confirmed by genetic

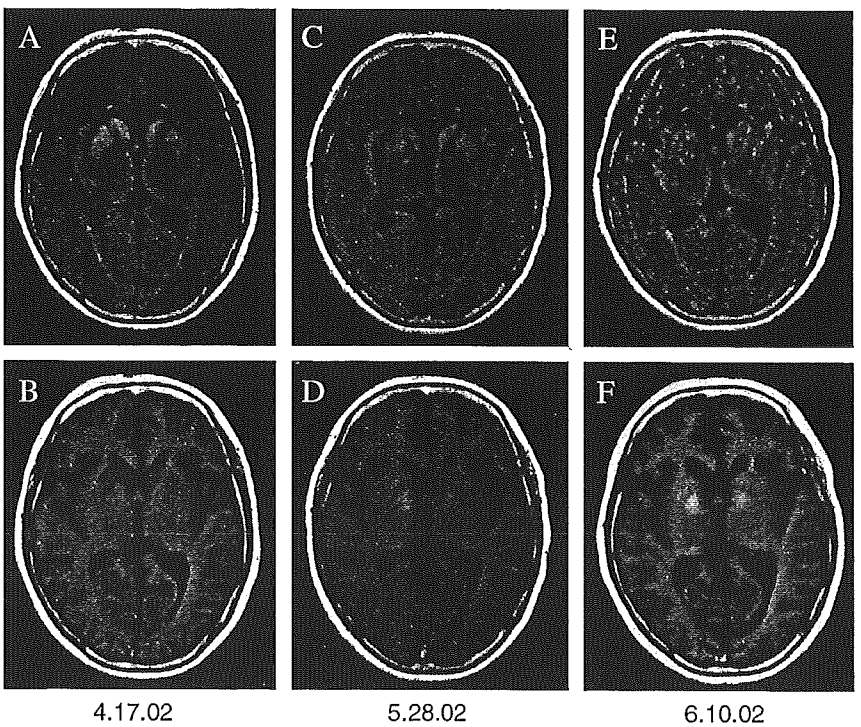

Fig. 2. Magnetic resonance imaging of the brain with serial fluid-attenuated inversion recovery (FLAIR) and T1-weighted imaging (T1WI). (A) and (B) were performed at admission, (C) and (D) at approximately 1 month, and (E) and (F) at 2 months after admission. (A) Hyperintense signals in the bilateral basal ganglia on FLAIR image. (B) Normal T1WI. (C) Slightly decreased hyperintense signals in the bilateral basal ganglia on FLAIR image. (D) Bilateral spotty hyperintense signals in the globus pallidus on T1WI. (E) No significant signal change in FLAIR (compared with FLAIR image at 1 month), but artifact prevented precise evaluation. (F) Increased signal intensity in the globus pallidus on T1WI (more apparent than at 1 month).

study in our patient. As has also been reported for other patients with this mutation [10,12–17], progression was more aggressive in our patient than in those with sporadic CJD. However, most clinical features of our case were similar to those of sporadic CJD, including rapidly progressive ataxia, severe mental deterioration, myoclonus, and typical periodic sharp-wave activity on EEG approximately 4 months after the onset of symptoms.

DWI abnormalities in our patient were observed as areas of high signal intensity in the putamen and caudate nucleus and as ribbon-like areas of hyperintensity in the cortical areas, predominantly in the insula, cingulate gyrus, and temporoparietal lobe. Although corresponding FLAIR images showed some hyperintensity in the basal ganglia, ADC mapping performed at the same time showed reduced signals in the corresponding regions, indicating that T2 shine-through contributed to the hyperintensity in the DWI only to a slight degree. The abnormalities found in our patient resemble those observed in sporadic CJD [19–28], demonstrating that similar MRI abnormalities can be found in both forms of the disease.

DWI appears to be a valuable tool that should be included in the diagnostic criteria for CJD [33]. Marked DWI changes can be observed in the early stages of symptomatic onset and are sustained over several months, although the high signal intensity seen on DWI may disappear over time in patients with advanced sporadic CJD (unpublished data). Shiga et al. [33] concluded that DWI was a more sensitive test for the early clinical diagnosis of CJD than periodic sharp wave complexes on EEG, detection of CSF 14–3–3 protein, or increase of NSE in the CSF. DWI may detect areas of increased signal intensity in the basal ganglia and cerebral cortex with greater sensitivity than that of routine MRI sequences such as T1WI, T2WI, or FLAIR images [18,34].

The pathogenesis of DWI abnormalities in the basal ganglia and cerebral cortex in CJD is not well understood. Spongiform neuronal degeneration and microglial activation might contribute to the changes demonstrated on DWI [35,36]. Cambier et al. [37] have suggested that high signal intensity on DWI may be related to periodic sharp-wave complex discharges on EEG. The EEG did not show specific changes corresponding to the DWI abnormalities in our case. Although our patient showed positive 14–3–3 protein and increased NSE in the CSF, as in sporadic CJD, it is unclear whether these findings are also related to the DWI abnormalities.

T1WI signals in the globus pallidus were initially normal in our patient and increased in intensity bilaterally during the early stages. This phenomenon might represent rapid pathologic changes in the basal ganglia during the course of the illness, corresponding to the hyperintensities shown on DWI. Such changes have previously been reported in only 1 patient with sporadic CJD, who showed typical clinical characteristics [38]. Although the high T1WI signal intensity in the globus pallidus may have been due to accumulation of prion protein in the brain [38], increased metal concentration can also cause high signal intensity on T1WI [39]. It remains doubtful whether T1WI abnormalities are pathognomonic for either sporadic or familial CJD.

To our knowledge, this is the first report to of MRI showing DWI and T1WI abnormalities in familial CJD with a point mutation at codon 200. Despite the clinical diversity and atypical laboratory findings seen in familial CJD with the codon 200 mutation, these neuroimaging studies suggest that common regional distributions and a common pathogenesis might underlie the clinical progression in both sporadic and familial CJD with the codon 200 mutation in the prion protein gene. Thus, DWI abnormalities may be characteristic features that should be considered in the diagnosis of familial as well as of sporadic CJD.

References

[1] Brown P, Cathala F, Castaigne P, Gajdusek DC. Creutzfeldt–Jakob disease: clinical analysis of a consecutive series of 230 neuropathologically verified cases. Ann Neurol 1986;20:597–602.
[2] Johnson RT, Gibbs CJ. Creutzfeldt–Jakob disease and related transmissible spongiform encephalopathies. N Engl J Med 1998;339:1994–2004.
[3] Richardson EP, Masters CL. The nosology of Creutzfeldt–Jakob disease and conditions related to the accumulation of PrP^{CJD} in the nervous system. Brain Pathol 1995;5:33–41.
[4] Masters CL, Harris JO, Gajdusek DC, Gibbs Jr CJ, Bernoulli C, Asher DM. Creutzfeldt–Jakob disease: patterns of worldwide occurrence and the significance of familial and sporadic clustering. Ann Neurol 1979;5:177–88.
[5] Zerr I, Pocchiari M, Collins S, Brandel JP, de Pedro Cuesta J, Knight RS, et al. Analysis of EEG and CSF 14–3–3 proteins as aids to the diagnosis of Creutzfeldt–Jakob disease. Neurology 2000;55:811–5.
[6] Zerr I, Bodemer M, Gefeller O, Otto M, Poser S, Wiltfang J, et al. Detection of 14–3–3 protein in the cerebrospinal fluid supports the diagnosis of Creutzfeldt–Jakob disease. Ann Neurol 1998;43:32–40.
[7] Hsich G, Kenney K, Gibbs CJ, Lee KH, Harrington MG. The 14–3–3 brain protein in cerebrospinal fluid as a marker for transmissible spongiform encephalopathies. N Engl J Med 1996;335:924–30.
[8] Aksamit Jr AJ, Preissner CM, Homburger HA. Quantitation of 14–3–3 and neuron-specific enolase proteins in CSF in Creutzfeldt–Jakob disease. Neurology 2001;57:728–30.
[9] Brandel JP, Delasnerie-Laupretre N, Laplanche JL, Hauw JJ, Alperovitch A. Diagnosis of Creutzfeldt–Jakob disease: effect of clinical criteria on incidence estimates. Neurology 2000;54:1095–9.
[10] Seno H, Tashiro H, Ishino H, Inagaki T, Nagasaki M, Morikawa S. New haplotype of familial Creutzfeldt–Jakob disease with a codon 200 mutation and a codon 219 polymorphism of the prion protein gene in a Japanese family. Acta Neuropathol (Berl) 2000;99:125–30.
[11] Hauw JJ, Sazdovitch V, Laplanche JL, Peoc'h K, Kopp N, Kemeny J, et al. Neuropathologic variants of sporadic Creutzfeldt–Jakob disease and codon 129 of PrP gene. Neurology 2000;54:1641–6.
[12] Meiner Z, Gabizon R, Prusiner SB. Familial Creutzfeldt–Jakob disease. Codon 200 prion disease in Libyan Jews. Medicine (Baltimore) 1997;76:227–37.
[13] Iwabuchi K, Endoh S, Hagimoto H, Okamoto K, Miyakawa T, Yamaguchi T, et al. Three patients from two families with familial Creutzfeldt–Jakob disease having a point mutation in the prion protein gene at codon 200 (Glu→Lys). No To Shinkei 1994;46:349–54.
[14] Kawauchi Y, Okada M, Kuroiwa Y, Ishihara O, Akai J. Familial Creutzfeldt–Jakob disease with the heterozygous point mutation at

codon 200 of the prion protein gene (Glu→Lys)–report of CJD200 brothers of Yamanashi Prefecture origin. No To Shinkei 1997;49: 460–4.
[15] Salvatore M, Pocchiari M, Cardone F, Petraroli R, D'Alessandro M, Galvez S, et al. Codon 200 mutation in a new family of Chilean origin with Creutzfeldt–Jakob disease. J Neurol Neurosurg Psychiatry 1996; 61:111–2.
[16] Chapman J, Arlazoroff A, Goldfarb LG, Cervenakova L, Neufeld MY, Werber E, et al. Fatal insomnia in a case of familial Creutzfeldt–Jakob disease with the codon 200 (Lys) mutation. Neurology 1996; 46:758–61.
[17] Antoine JC, Laplanche JL, Mosnier JF, Beaudry P, Chatelain J, Michel D. Demyelinating peripheral neuropathy with Creutzfeldt–Jakob disease and mutation at codon 200 of the prion protein gene. Neurology 1996;46:1123–7.
[18] Mendez OE, Shang J, Jungreis CA, Kaufer DI. Diffusion-weighted MRI in Creutzfeldt–Jakob disease: a better diagnostic marker than CSF protein 14–3–3? J Neuroimaging 2003;13:147–51.
[19] Bahn MM, Kido DK, Lin W, Pearlman AL. Brain magnetic resonance diffusion abnormalities in Creutzfeldt–Jakob disease. Arch Neurol 1997;54:1411–5.
[20] Bahn MM, Parchi P. Abnormal diffusion-weighted magnetic resonance images in Creutzfeldt–Jakob disease. Arch Neurol 1999;56: 577–83.
[21] Demaerel P, Baert AL, Vanopdenbosch L, Robberecht W, Dom R. Diffusion-weighted magnetic resonance imaging in Creutzfeldt–Jakob disease. Lancet 1997;349:847–8.
[22] Demaerel P, Heiner L, Robberecht W, Sciot R, Wilms G. Diffusion-weighted MRI in sporadic Creutzfeldt–Jakob disease. Neurology 1999;52:205–8.
[23] Demaerel P, Sciot R, Robberecht W, Dom R, Vandermeulen D, Maes F, et al. Accuracy of diffusion-weighted MR imaging in the diagnosis of sporadic Creutzfeldt–Jakob disease. J Neurol 2003;250:222–5.
[24] Matoba M, Tonami H, Miyaji H, Yokota H, Yamamoto I. Creutzfeldt–Jakob disease: serial changes on diffusion-weighted MRI. J Comput Assist Tomogr 2001;25:274–7.
[25] Na DL, Suh CK, Choi SH, Moon HS, Seo DW, Kim SE, et al. Diffusion-weighted magnetic resonance imaging in probable Creutzfeldt–Jakob disease: a clinical–anatomic correlation. Arch Neurol 1999;56:951–7.
[26] Nagaoka U, Kurita K, Hosoya T, Kitamoto T, Kato T. Diffusion images on brain MRI in Creutzfeldt–Jakob disease. Clin Neurol 1999;39:468–70.
[27] Schaefer PW, Grant PE, Gonzalez RG. Diffusion-weighted MR imaging of the brain. Radiology 2000;217:331–45.
[28] Yee AS, Simon JH, Anderson CA, Sze CI, Filley CM. Diffusion-weighted MRI of right-hemisphere dysfunction in Creutzfeldt–Jakob disease. Neurology 1999;52:1514–5.
[29] Nitrini R, Mendonca RA, Huang N, LeBlanc A, Livramento JA, Marie SK. Diffusion-weighted MRI in two cases of familial Creutzfeldt–Jakob disease. J Neurol Sci 2001;184:163–7.
[30] Ishida S, Sugino M, Koizumi N, Shinoda K, Ohsawa N, Ohta T, et al. Serial MRI in early Creutzfeldt–Jacob disease with a point mutation of prion protein at codon 180. Neuroradiology 1995;37:531–4.
[31] Huang N, Marie SK, Kok F, Nitrini R. Familial Creutzfeldt–Jakob disease associated with a point mutation at codon 210 of the prion protein gene. Arq Neuropsiquiatr 2001;59:932–5.
[32] Satoh A, Goto H, Satoh H, Tomita I, Seto M, Furukawa H, et al. A case of Creutzfeldt–Jakob disease with a point mutation at codon 232: correlation of MRI and neurologic findings. Neurology 1997;49: 1469–70.
[33] Shiga Y, Miyazawa K, Sato S, Fukushima R, Shibuya S, Sato Y, et al. Diffusion-weighted MRI abnormalities as an early diagnostic marker for Creutzfeldt–Jakob disease. Neurology 2004;6:443–9.
[34] Mendez OE, Shang J, Jungreis CA, Kaufer DI. Accuracy of diffusion-weighted MR imaging in the diagnosis of sporadic Creutzfeldt–Jakob disease. J Neurol 2003;250:222–5.
[35] Bergui M, Bradac GB, Rossi G, Orsi L. Extensive cortical damage in a case of Creutzfeldt–Jacob disease: clinicoradiological correlations. Neuroradiology 2003;45:304–7.
[36] Mittal S, Farmer P, Kalina P, Kingsley PB, Halperin J. Correlation of diffusion-weighted magnetic resonance imaging with neuropathology in Creutzfeldt–Jakob disease. Arch Neurol 2002;59:128–34.
[37] Cambier DM, Kantarci K, Worrell GA, Westmoreland BF, Aksamit AJ. Lateralized and focal clinical, EEG, and FLAIR MRI abnormalities in Creutzfeldt–Jakob disease. Clin Neurophysiol 2003;114: 1724–8.
[38] de Priester JA, Jansen GH, de Kruijk JR, Wilmink JT. New MRI findings in Creutzfeldt–Jakob disease: high signal in the globus pallidus on T1-weighted images. Neuroradiology 1999;41:265–8.
[39] Maeda H, Sato M, Yoshikawa A, Kimura M, Sonomura T, Terada M, et al. Brain MR imaging in patients with hepatic cirrhosis: relationship between high intensity signal in basal ganglia on T1-weighted images and elemental concentrations in brain. Neuroradiology 1997;39:546–50.

Neuropathology and Applied Neurobiology (2005), **31**, 80–87 doi: 10.1111/j.1365-2990.2004.00592.x

Fatal familial insomnia with an unusual prion protein deposition pattern: an autopsy report with an experimental transmission study

K. Sasaki*, K. Doh-ura*, Y. Wakisaka*, H. Tomoda† and T. Iwaki*

**Department of Neuropathology, Neurological Institute, Graduate School of Medical Sciences, Kyushu University, Fukuoka, and †Department of Neurology, Imazu Red Cross Hospital, Imazu, Fukuoka, Japan*

K. Sasaki, K. Doh-ura, Y. Wakisaka, H. Tomoda and T. Iwaki (2005) *Neuropathology and Applied Neurobiology* 31, 80–87

Fatal familial insomnia with an unusual prion protein deposition pattern: an autopsy report with an experimental transmission study

We recently performed a *post-mortem* examination on a Japanese patient who had a prion protein gene mutation responsible for fatal familial insomnia (FFI). The patient initially developed cerebellar ataxia, but finally demonstrated insomnia, hyperkinetic delirium, autonomic signs and myoclonus in the late stage of the illness. Histological examination revealed marked neuronal loss in the thalamus and inferior olivary nucleus; however, prion protein (PrP) deposition was not proved in these lesions by immunohistochemistry. Instead, PrP deposition and spongiform change were both conspicuous within the cerebral cortex, whereas particular PrP deposition was also observed within the cerebellar cortex. The abnormal protease-resistant PrP (PrP^{res}) molecules in the cerebral cortex of this case revealed PrP^{res} type 2 pattern and were compatible with those of FFI cases, but the transmission study demonstrated that a pathogen in this case was different from that in a case with classical FFI. By inoculation with homogenate made from the cerebral cortex, the disease was transmitted to mice, and neuropathological features that were distinguishable from those previously reported were noted. These findings indicate the possibility that a discrete pathogen was involved in the disease in this case. We suggest that not only the genotype of the PrP gene and some other as yet unknown genetic factors, but also the variation in pathogen strains might be responsible for the varying clinical and pathological features of this disease.

Keywords: Creutzfeldt-Jakob disease, NZW mouse, prion disease, thalamic form, transmissible spongiform encephalopathy

Introduction

Fatal familial insomnia (FFI) is one of the disease entities of prion disease or transmissible spongiform encephalopathy (TSE) and it is linked to a mutation at codon 178 of the prion protein gene (PRNP), aspartic acid to asparagine substitution (D178N), in conjunction with methionine at the polymorphic position 129 of the mutant allele [1]. The neuropathological hallmark of FFI is the predominance of lesions within the thalamus [2]. Clinically this disorder is characterized by progressive insomnia, dysautonomia and motor signs [3]. The D178N mutation is also associated with familial Creutzfeldt-Jakob disease (CJD). The disease phenotypes have been considered to depend on the polymorphism at codon 129 of the mutant allele, methionine (129Met) in FFI and valine (129Val) in CJD [4]. However, the FFI genotype reveals diverse clinical expression including cerebellar ataxia, dementia and autonomic abnormalities with or without insomnia [5,6]. In Japan, one FFI case [7] and some cases of the 'sporadic'

Correspondence: Kensuke Sasaki, Department of Neuropathology, Neurological Institute, Graduate School of Medical Sciences, Kyushu University, Fukuoka 812-8582, Japan. Tel: +81-92-6425539; Fax: +81-92-6425540; E-mail: ksasaki@np.med.kyushu-u.ac.jp

thalamic form of CJD [8,9] have been reported, and these have indicated a discrepancy between PRNP genotype and the disease phenotype.

We recently performed a *post-mortem* examination on a Japanese patient with a 27-month history of familial prion disease with PRNP D178N-129Met mutation. The clinical data on this patient and his family have been published in part [10]. Here we report additional clinical data and *post-mortem* neuropathological findings, as well as findings in mice infected with the patient's material.

Case report

The pedigree is presented in Figure 1. In October 1997, a 50-year-old Japanese man (Patient II-5) developed an unsteady gait, followed within a month by difficulty in speech. Although these symptoms worsened rapidly, he did not immediately develop either dementia or insomnia. He was admitted to a hospital for neurological evaluation in February 1998, and PRNP D178N-129Met mutation (heterozygous for 129Met/Val) was revealed as previously reported [10]. From October 1998, either insomnia or delirium was clearly apparent. Hyperthermia without any signs indicative of infection or inflammation, thus suggesting an autonomic sign, was also observed. He often showed reality disturbance and restlessness. He became progressively demented, developed trismus, myoclonus and horizontal nystagmus, and demonstrated increased muscle tone. Finally he became bedridden with flexion contracture. Brain computed tomography revealed mild atrophy of the cerebellum and brainstem. Electroencephalograms showed a background of 9 Hz diffuse α activities, but periodic synchronous discharges were not detected during the clinical course. Sleep activities with rapid eye movements were not recorded in sleep electroencephalograms. In January 2000, he died of pneumonia at the age of 52 years, about 27 months after the onset of disease.

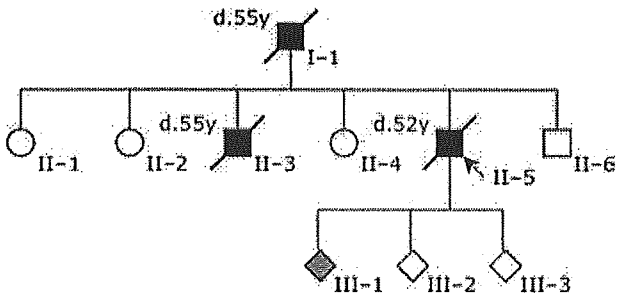

Figure 1. Family tree of the present pedigree. Patients who developed rapidly progressive cerebellar ataxia are depicted by closed symbols, along with their age at death (years old). One of the children of the present case has fatal familial insomnia genotype D178N-129Met/Met (grey symbol).

Patient II-3, one of the brothers of Patient II-5, also showed rapidly progressive cerebellar ataxia. He developed an ataxic gait, forgetfulness and dysarthria at the age of 55 years. Brain computed tomography demonstrated moderate cerebellar atrophy, and electroencephalograms showed diffuse intermittent slow activities without periodic synchronous discharges. He developed myoclonic jerks, akinetic mutism with a decorticate posture, and died 7 months after the onset. Patient I-1, the father of Patients II-5 and II-3, had also developed an ataxic gait and dementia at the age of 55 years. He died of unknown causes after a clinical course of 12 months. Neither autopsy nor PRNP analysis was carried out in either Patient I-1 or Patient II-3. One of the children of Patient II-5 was revealed to have PRNP D178N-129Met mutation (homozygous for 129Met).

Materials and methods

Autopsy was performed 6 h *post-mortem*. A frontal tip of the right cerebral hemisphere and a cerebellar tip were sampled and frozen for Western blot analysis. The remaining brain was immersion-fixed in 10% formalin for 2 weeks. Tissue blocks were immersed in 98% formic acid for 1 h and paraffin-embedded. Hematoxylin and eosin (HE) stain, Klüver-Barrera stain and Bodian's method were performed on 7-μm-thick sections. Immunohistochemical analyses were performed by a standard indirect method for glial fibrillary acidic protein (GFAP) (polyclonal, Dako, Denmark, or monoclonal, clone G-A-5, Roche, Switzerland), ferritin (polyclonal, Dako), β-amyloid precursor protein (APP) (monoclonal, clone LN27, Zymed, USA), SNAP-25 (monoclonal, clone MAB331, Chemicon, USA) and prion protein (PrP) (monoclonal, clone 3F4, Senetek, USA). For anti-PrP immunohistochemistry, sections were pretreated with hydrolytic autoclaving as previously reported [11]. Western blot analysis for protease-resistant PrP (PrP^{res}) was performed using frontal cortical and cerebellar tissue tips from this case, applying phosphotungstic acid precipitation of PrP^{res} as described previously [12] with 50 μg/ml proteinase K (PK) digestion, along with a control case with sporadic

CJD (77-year-old man, duration of illness was 9 months, 129Met/Met). Transmission study was performed as described previously [13]. Briefly, frontal cortical tissue tips were aseptically homogenized with nine volumes of saline, and after removal of debris by low-speed centrifugation the supernatant was used as 10% homogenate. Twenty microliters of 10% homogenate were injected intracerebrally into female NZW mice or female Tg7 mice expressing hamster PrP but not endogenous murine PrP. Sections of infected mice were analysed by HE stain and also by immunohistochemistry for PrP (polyclonal, PrP-C, IBL, Japan) and GFAP (clone G-A-5, Roche). Permission for the animal experiments was obtained from the Animal Experiment Committee of Kyushu University.

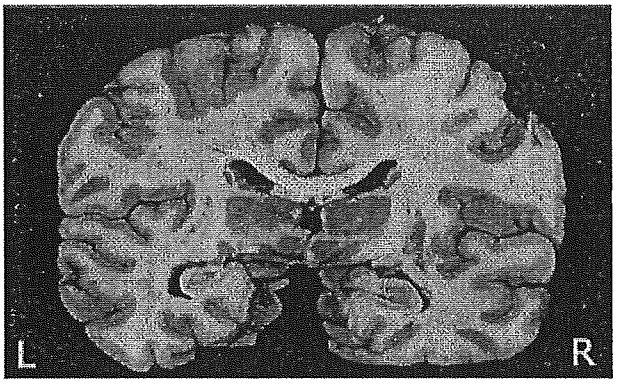

Figure 2. Coronal section at the thalamic level. The medial part of the thalamus is atrophic and the third ventricle is dilated.

Results

The brain weighed 1350 g before fixation. The cerebellum showed slight atrophy, whereas the volume of the forebrain was preserved. Coronal sections showed atrophy of the medial part of the thalamus and symmetrical dilatation of the third ventricle (Figure 2).

The summary of histological examination is shown in Figure 3. Marked neuronal loss and moderate astrogliosis in the thalamus were observed, most prominently in its centromedial nucleus and dorsomedial nucleus. However, spongiform change was imperceptible (Figure 4A,B). Neuronal loss and gliosis in the medial portion of the inferior olivary nucleus were also apparent (Figure 4C,D). In the cerebellum there was mild loss of granular cells, and the molecular layer was slightly atrophic. There were localized lesions of spongiosis in the cerebellar molecular layer. Purkinje's cells appeared not to be decreased in number, but they often demonstrated shrunken features. The cerebellar white matter showed diffuse myelin pallor. The cerebral cortex showed uneven distribution of spongiform change and neuronal loss (Figure 4E). There was no apparent difference in the intensities of the cortical lesions among the lobes of the cerebrum except that the lesions are more prominent in the entorhinal cortex and less in the occipital lobe. Moderate astrogliosis was associated with the spongiform lesions (Figure 4F).

Immunohistochemistry for PrP revealed that there was no punctate or plaque-type immunoreactivity in the thal-

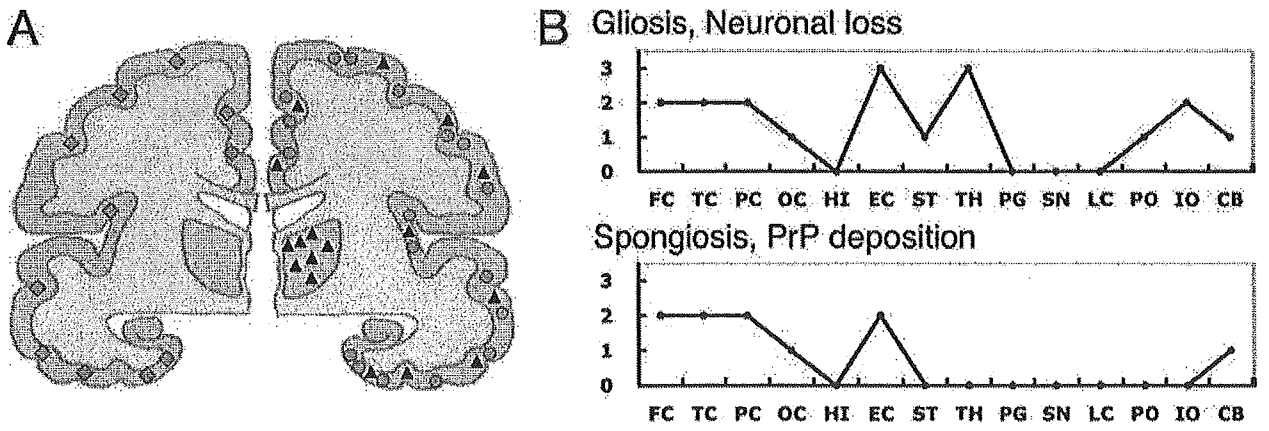

Figure 3. Lesion profiles of the present case. A: schematic drawing of the distribution of prion protein (PrP) deposition (diamonds), spongiosis (circles) and neuronal loss (triangles) in this case, which can be compared to that of fatal familial insomnia (FFI) and 178CJD shown in ref. [19]. B: lesion profiles in respect to gliosis/neuronal loss and spongiosis/PrP deposition. Brain regions studied were: frontal cortex (FC), temporal cortex (TC), parietal cortex (PC), occipital lobe (OC), hippocampus (HI), entorhinal cortex (EC), striatum (ST), thalamus (TH), substantia nigra (SN), periaqueductal grey (PG), pons (PO), locus ceruleus (LC), medulla oblongata (ME), cerebellum (CB). The vertical axis is the degree of lesion graded as follows. 0: not detectable; 1: mild; 2: moderate; 3: severe.